V.A.4 Performance of Automotive Fuel Cell Systems with Low-Pt Nanostructured Thin Film Catalysts at High Power Densities

Rajesh K. Ahluwalia (Primary Contact),
Xiaohua Wang, Romesh Kumar

Argonne National Laboratory
9700 South Cass Avenue
Argonne, IL 60439
Phone: (630) 252-5979
Email: walia@anl.gov

DOE Manager
HQ: Nancy Garland
Phone: (202) 586-5673
Email: Nancy.Garland@ee.doe.gov

Project Start Date: October 1, 2003
Project End Date: Project continuation and direction
determined annually by DOE

Fiscal Year (FY) 2012 Objectives

- Develop a validated model for automotive fuel cell systems, and use it to assess the status of the technology.
- Conduct studies to improve performance and packaging, to reduce cost, and to identify key research and development (R&D) issues.
- Compare and assess alternative configurations and systems for transportation and stationary applications.
- Support DOE/United States Driving Research and Innovation for Vehicle efficiency and Energy sustainability automotive fuel cell development efforts.

Technical Barriers

This project addresses the following technical barriers from the Fuel Cells section of the Fuel Cell Technologies Program Multi-Year Research, Development and Demonstration Plan:

(B) Cost
(C) Performance

Technical Targets

This project is conducting system level analyses to address the following DOE 2015 technical targets for automotive fuel cell power systems operating on direct hydrogen:

- Energy efficiency: 50%-60% (55%-65% for stack) at 100%-25% of rated power
- Power density: 650 W/L for system, 2,000 W/L for stack

- Specific power: 650 W/kg for system, 2,000 W/kg for stack
- Transient response: 1 s from 10% to 90% of rated power
- Start-up time: 30 s from -20°C and 5 s from $+20^{o}$C ambient temperature
- Precious metal content: 0.2 g/kW

FY 2012 Accomplishments

- Collaborated with 3M in taking cell data to validate the model for nanostructured thin-film catalyst-based membrane electrode assembly (MEA) and stacks.
- Formulated a hybrid model combining theory for reversible potentials and electrode kinetics and neural network for mass transfer overpotentials.
- Conducted a single-variable optimization study to determine the optimum stack temperatures and inlet relative humidities (RHs) for different stack inlet pressures, cathode stoichiometry, Pt loading in cathode, and system efficiency.
- Conducted a multi-variable optimization study to determine the optimum stack temperatures, inlet RHs, cathode stoichiometry and Pt loading for specified stack inlet pressure and system efficiency.

✧ ✧ ✧ ✧ ✧

Introduction

While different developers are addressing improvements in individual components and subsystems in automotive fuel cell propulsion systems (i.e., cells, stacks, balance-of-plant components), we are using modeling and analysis to address issues of thermal and water management, design-point and part-load operation, and component-, system-, and vehicle-level efficiencies and fuel economies. Such analyses are essential for effective system integration.

Approach

Two sets of models are being developed. The GCtool software is a stand-alone code with capabilities for design, off-design, steady-state, transient, and constrained optimization analyses of fuel cell systems (FCSs). A companion code, GCtool-ENG, has an alternative set of models with a built-in procedure for translation to the MATLAB®/SIMULINK platform commonly used in vehicle simulation codes, such as Autonomie.

Results

In FY 2012, we collaborated with 3M to obtain reference performance data on eight 50-cm^2 active area single-cell fixtures from Fuel Cell Technologies with serpentine flow fields. The MEAs consisted of 3M 24-μm membrane (850 equivalent weight), ternary $Pt_{0.68}Co_{0.3}Mn_{0.02}$ nanostructured thin-film catalyst (NSTFC), and 3M gas diffusion layers made by applying a hydrophobic treatment to a backing paper and a micro-porous layer [1]. All cells had a Pt loading of 0.050 mg·cm^{-2} in the anode. Two of the eight cells had a Pt loading of 0.103 mg·cm^{-2} in the cathode. The Pt loading in the cathode in the other cells (two each) was 0.054, 0.146 and 0.186 mg·cm^{-2}. All cells were first conditioned using a "thermal cycling" process, described in detail in Steinbach et al. [2], which consisted of repeated temperature and voltage cycles over a period of 2-3 days until stable performance was reached. The polarization curves were obtained on these cells for different temperatures (30-90°C), inlet pressures (1-2.5 atm), inlet RHs (25-100%), and stoichiometries for the cathode (1.5-10) and the anode (1.2-5) by running galvanodynamic scans at cell current densities varying from 0.02 to 2 A·cm^{-2}. The cell was held for 120 s at each current step and the cell voltage and the high-frequency resistance (from alternating current impedance measurements) were recorded every 5 s. Prior to the start of the experiments, for each cell, the electrochemical surface area (ECSA) was determined by cyclic voltammetry, the hydrogen crossover current density and cell short resistance were determined by measuring the plateau currents, and the mass activity of Pt was measured in H_2/O_2 at 80°C, 1-atm reactant H_2 and O_2 pressures, and 100% RH.

We used the measured polarization curves, high-frequency resistances, mass activities, ECSAs, and H_2 crossover current density to develop, train, and validate a multi-nodal hybrid fuel cell model combining the theory for reversible potentials and kinetic overpotentials for the oxygen reduction reaction (ORR) with an artificial neural network for mass transfer and ohmic overpotentials. The Nernst equation was used to determine the reversible potential as a function of the cell temperature and the partial pressures of H_2, O_2, and water vapor in the anode and cathode flow fields. The polarization data at low current densities (<0.4 A·cm^{-2}) were analyzed to develop a Tafel equation for ORR kinetic overpotential as a function of the current density, temperature, O_2 partial pressure, and relative humidity [3]. Figure 1 shows good agreement between the modeled and measured polarization curves for one series of tests conducted by varying the operating conditions from their reference values: 1.5 atm, 80°C, 100% RH at cell exit, SR_c=SR_a=2, and 0.050(a) and 0.103(c) mg·cm^{-2} Pt loading. Similar good agreement was also obtained for other series of tests and the model accuracy was within the reproducibility of the polarization data.

The hybrid cell model was used to evaluate the performance of an NSTFC stack in an 80-kW$_{net}$ fuel cell system (see Refs. [4,5] for system configuration). As discussed elsewhere [5], the cells are identical to the ones described above except for the flow fields that are assumed to be stamped from thermally nitrided Fe-20Cr-4V alloy foils. The air management subsystem consists of a compressor-expander module (CEM) with an air and liquid-cooled motor, mixed axial and radial flow compressor, variable-nozzle radial inflow turbine, and airfoil bearings [6]. The fuel management subsystem includes a hybrid ejector-hydrogen pump to recirculate the spent anode gas. The water management subsystem includes a membrane humidifier for the cathode air and an air precooler. The system is designed to be water balanced, i.e., only the water produced in the stack is used for humidifying the feed gases. The dual-loop heat rejection subsystem has a high-temperature circuit for supplying coolant to the stack, and a low-temperature circuit for supplying coolant to the vehicle traction motor, CEM motor and air pre-cooler. The coolant in both circuits is aqueous ethylene glycol solution.

Figure 2 compares the modeled performance of the NSTFC stack in systems S2 and S1 with 1.5 atm and 2.5 atm stack inlet pressures, respectively. Some of the important stack and system parameters are: 47.5% net system efficiency on lower heating value basis, Pt loading (L_{Pt}) of 0.050 mg·cm^{-2} in the anode catalyst and 0.100 mg·cm^{-2} in the cathode catalyst, 10°C rise in coolant temperature across the stack (ΔT_c), anode and cathode stoichiometries of 2, and 71% CEM compressor and 73% CEM expander efficiencies. Figure 2 indicates that there is an optimum stack temperature (assumed to be 5°C higher than the coolant exit temperature) and inlet RH$_c$ (not shown) at which the Pt content (g.kW^{-1}) and the system cost are the lowest. Here, the system cost has been estimated using the correlations presented in Ref. [7]. The optimum stack temperature depends on the operating pressure, increasing from 75°C at 1.5-atm stack inlet pressure to 82°C at 2.5-atm stack inlet pressure. The Pt content is ~13% lower in S1 in spite of the higher CEM parasitic power, 9.6 kW vs. 5.1 kW for S2. Thus, the stack in S1 has to produce an additional 4.5 kW for the fixed 80 kW net power, and to operate at 34 mV higher cell voltage to achieve the specified 47.5% net system efficiency. The model indicates that the power density at the design point is ~19% higher for the stack in S1, 837 mW·cm^{-2} at 679 mV, compared to 705 mW·cm^{-2} at 645 mV for the stack in S2. At high-volume manufacturing, the estimated cost is $53.1 kW^{-1} for system S2 and $49.7 kW^{-1} for system S1; see Refs. [7,8] for all assumptions used in estimating these costs.

Figure 3 quantifies the effect of Pt loading in the cathode catalyst layer on Pt content and system cost for systems S1 and S2. Our results indicate that the stack power density increases less than linearly (668 to 979 mW·cm^{-2} in S1 and 620 to 760 W·cm^{-2} in S2) with the increase in
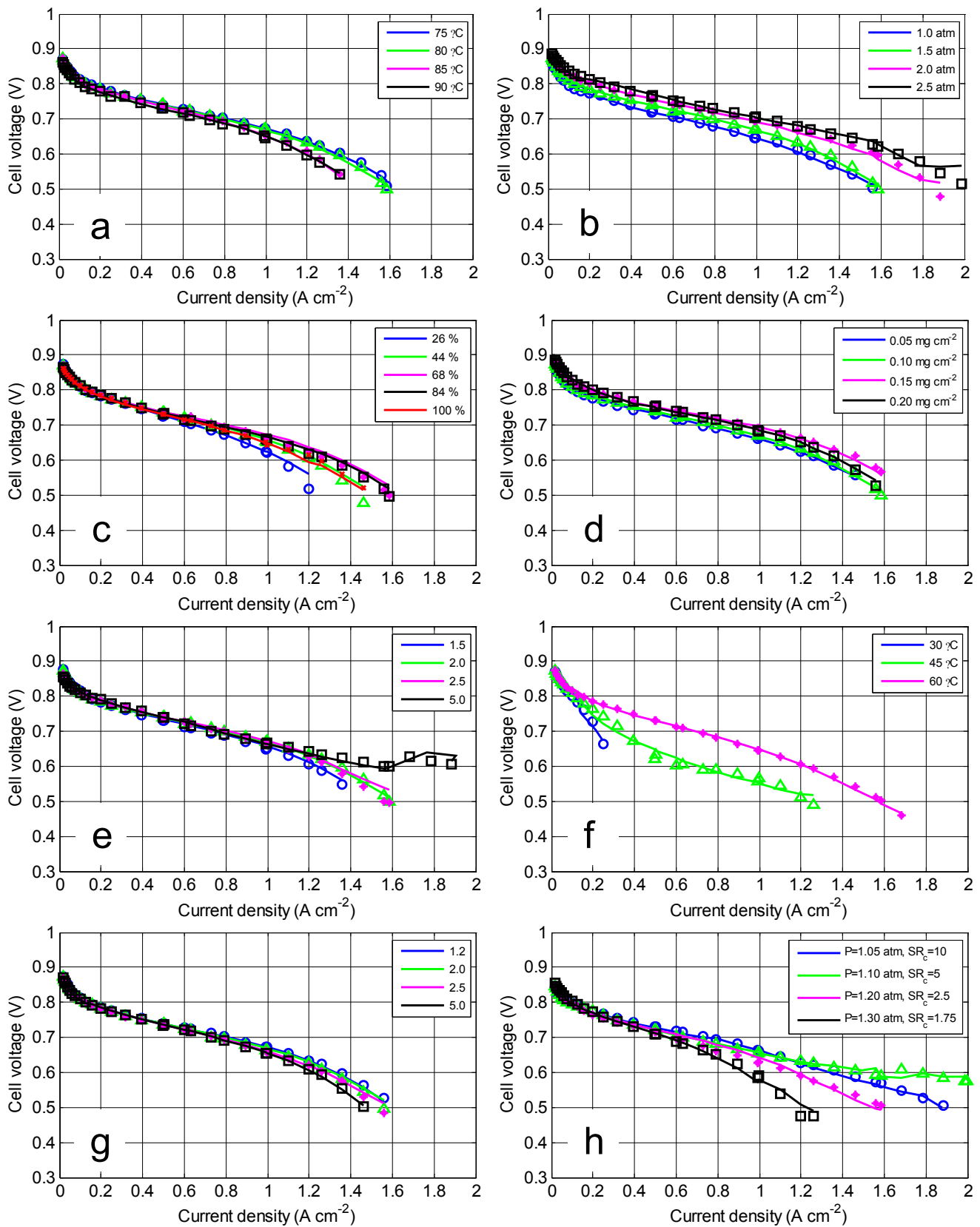
FIGURE 1. Validation of the hybrid fuel cell model using polarization curves for the cell with 0.1 mg.cm^{-2} Pt in the cathode catalyst. The variables are: a) cell temperature; b) inlet pressure; c) inlet relative humidity; d) cathode Pt loading; e) cathode stoichiometry; f) low temperature, g) anode stoichiometry; and h) low pressure and high cathode stoichiometry
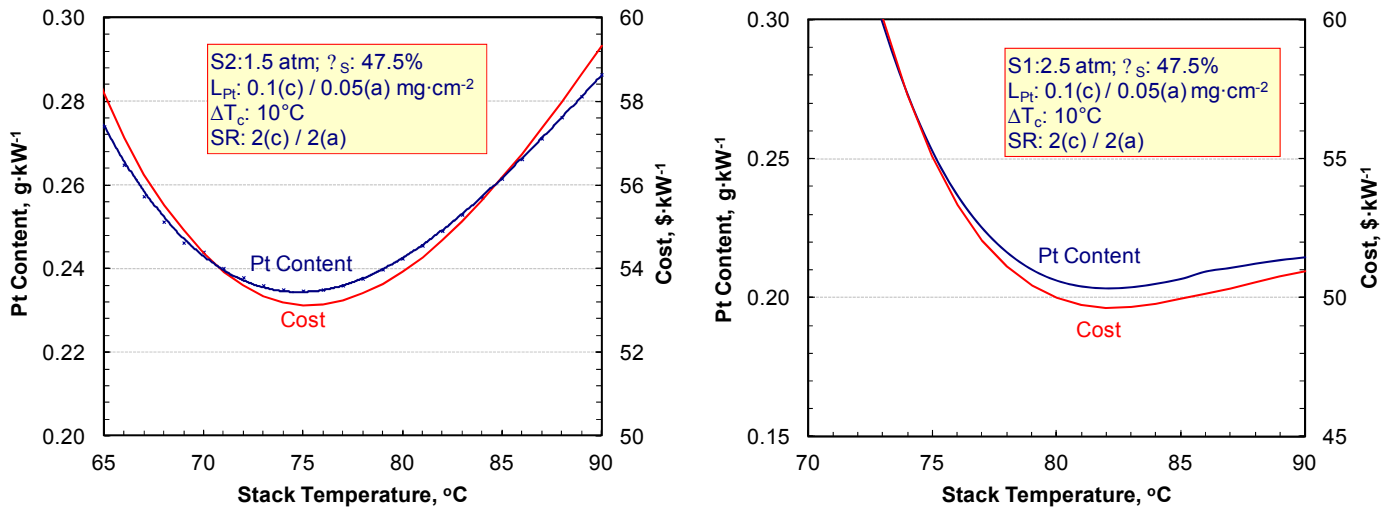
FIGURE 2. Effect of operating conditions on Pt content and system cost, 47.5% system efficiency
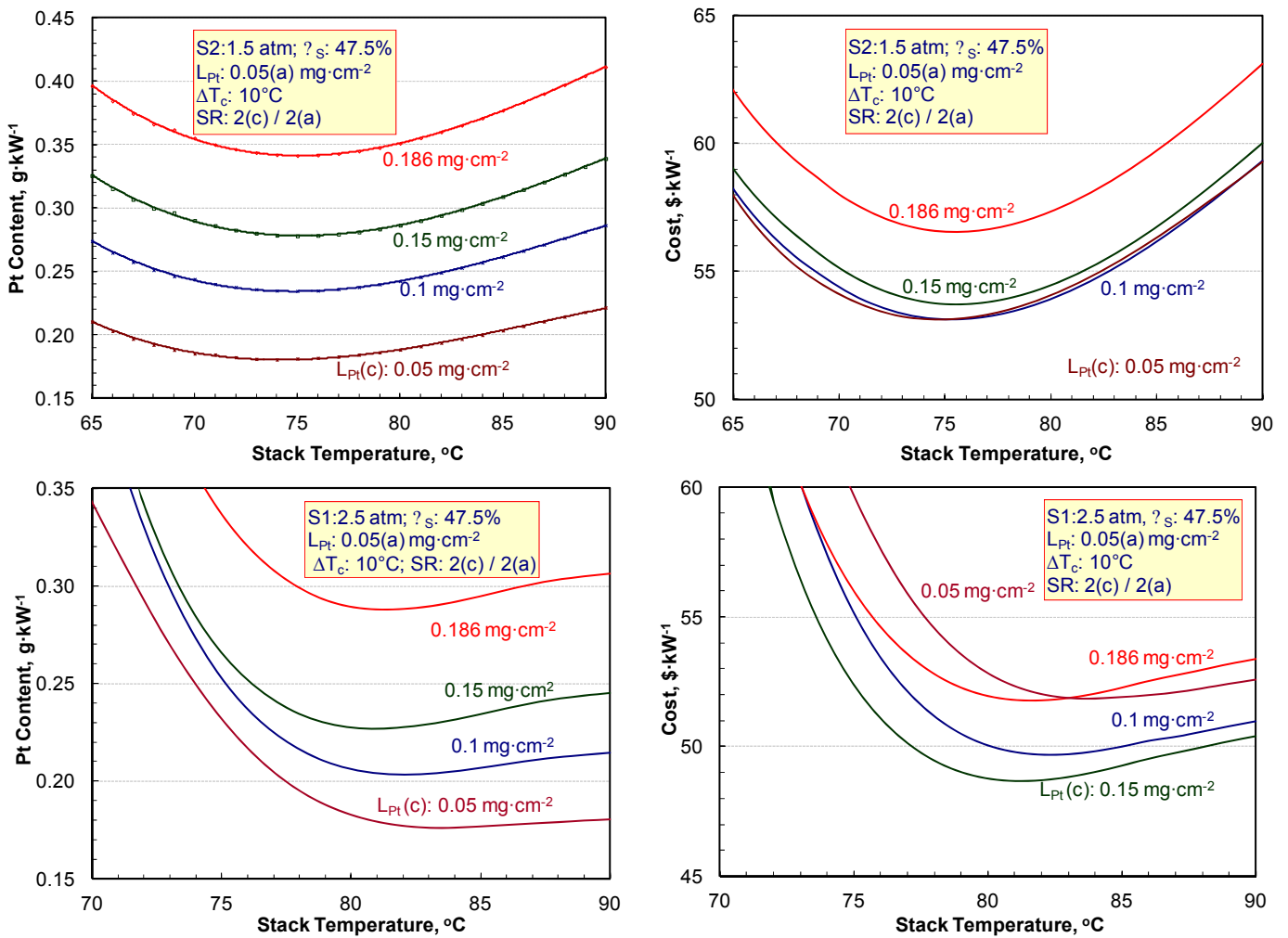

FIGURE 3. Effect of Pt loading in cathode catalyst on Pt content and system cost, 47.5% system efficiency

cathode Pt loading from 0.050 to 0.150 mg·cm^{-2}, and that it actually decreases if the Pt loading is increased beyond 0.150 mg·cm^{-2}. The optimum stack temperature shows a small increase as the Pt loading is reduced because of the temperature dependence of ORR activity. The lowest Pt loading (0.050 mg·cm^{-2}) in the cathode catalyst layer results in the smallest Pt content, in spite of the lowest stack power density. The stack and system costs are lowest for 0.150 mg·cm^{-2} Pt loading in cathode for system S1 and 0.050-0.100 mg·cm^{-2} Pt loading in cathode for system S2. At the optimum operating conditions and Pt loadings, the lowest system cost is \$48.8 kW^{-1} for system S1 and \$53.1 kW^{-1} for system S2, divided nearly equally between the stack (51.4% for system S1, 54.7-55,3% for system S2) and the balance-of-plant components (44.7-49.6%). Pt accounts for 16.5% of the system cost and 32.1% of the stack cost in system S1 and 12.1-15.6% of the system cost and 22.1-28.5% of the stack cost in system S2.

Figure 4 shows the effect of CEM performance on Pt content and system cost for system S1. The label "CEM-Map" in Figure 4 refers to 71% compressor, 73% expander, and 80% combined motor and controller efficiencies, as measured in laboratory tests, with additional losses due to air-foil bearings and motor cooling air. The label "CEM-Status" refers to the same component efficiencies but it is assumed that instead of venting the motor cooling air, it is combined with the compressed and humidified air before entering the stack. The label "CEM-Target" refers to 75% compressor, 80% expander and 85% combined motor and controller efficiencies, and a 10% allowance for other losses. The estimated CEM parasitic power is 11.1 kW$_e$ for CEM-Map, 9.6 kW$_e$ for CEM-Status and 7.9 kW$_e$ for CEM-Target. Figure 4 shows that, for fixed 47.5% system efficiency, a 1.7 kW$_e$ reduction in parasitic power (CEM-Status vs. CEM-Target)

translates to ~8.6% reduction in Pt content and ~3.8% saving in system cost.

Figure 5 summarizes results from a parametric study on the effect of cathode stoichiometry ratio (SR$_c$) on the performance of systems S2 and S1 for fixed system efficiency. The lower-pressure system S2 shows only a small benefit in lowering SR$_c$ from 2 to 1.5, implying that the benefit of reduced parasitic power is offset by the resulting decrease in stack power density. The higher-pressure system S1 shows a greater sensitivity of Pt content and system cost to SR$_c$. Figure 5 indicates that as SR$_c$ is lowered in system S1, the optimum stack temperature increases to prevent flooding of the cathode catalyst layer. At 2.5 atm stack inlet pressure, the advantage of reduced parasitic power at SR$_c$ of 1.5 more than compensates for the decrease in the stack power density.

Finally, we conducted an optimization study, in which the system cost was minimized by simultaneously varying the stack temperature (70-90°C), coolant ΔT (5-25°C), cathode Pt loading (0.1-0.2 mg·cm^{-2}), and inlet RH for specified stack inlet pressure (1.5-2.5 atm) and system efficiency (35-50%). The FCS net power (80 kW$_e$), cathode stoichiometry (1.5) and Pt loading in the anode catalyst (0.050 mg·cm^{-2}) were held constant. We found that the optimum Pt loading in the cathode is a function of stack inlet pressure and system efficiency, and it decreases as the value of either parameter is reduced. Both the Pt content and system cost decrease as the stack inlet pressure is increased. At 2.5 atm, the required cell voltage decreases by 43 mV (from 689 mV to 646 mV) if the target system efficiency is lowered from 50% to 45% with a resulting 29% reduction in Pt content and \$3.1 kW^{-1} saving in system cost. The lower the system efficiency, the cheaper is the stack, but more expensive are the BOP components. Thus, the cost saving is quite marginal and may be negative in system S1 if the
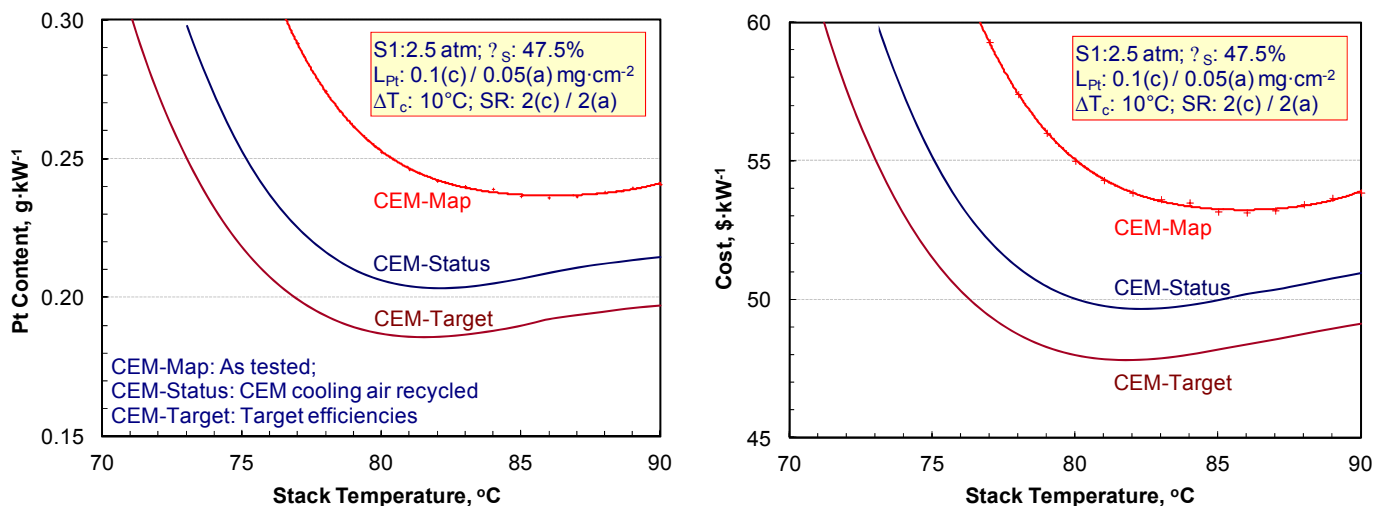

FIGURE 4. Effect of CEM performance on Pt content and system cost, 47.5% system efficiency
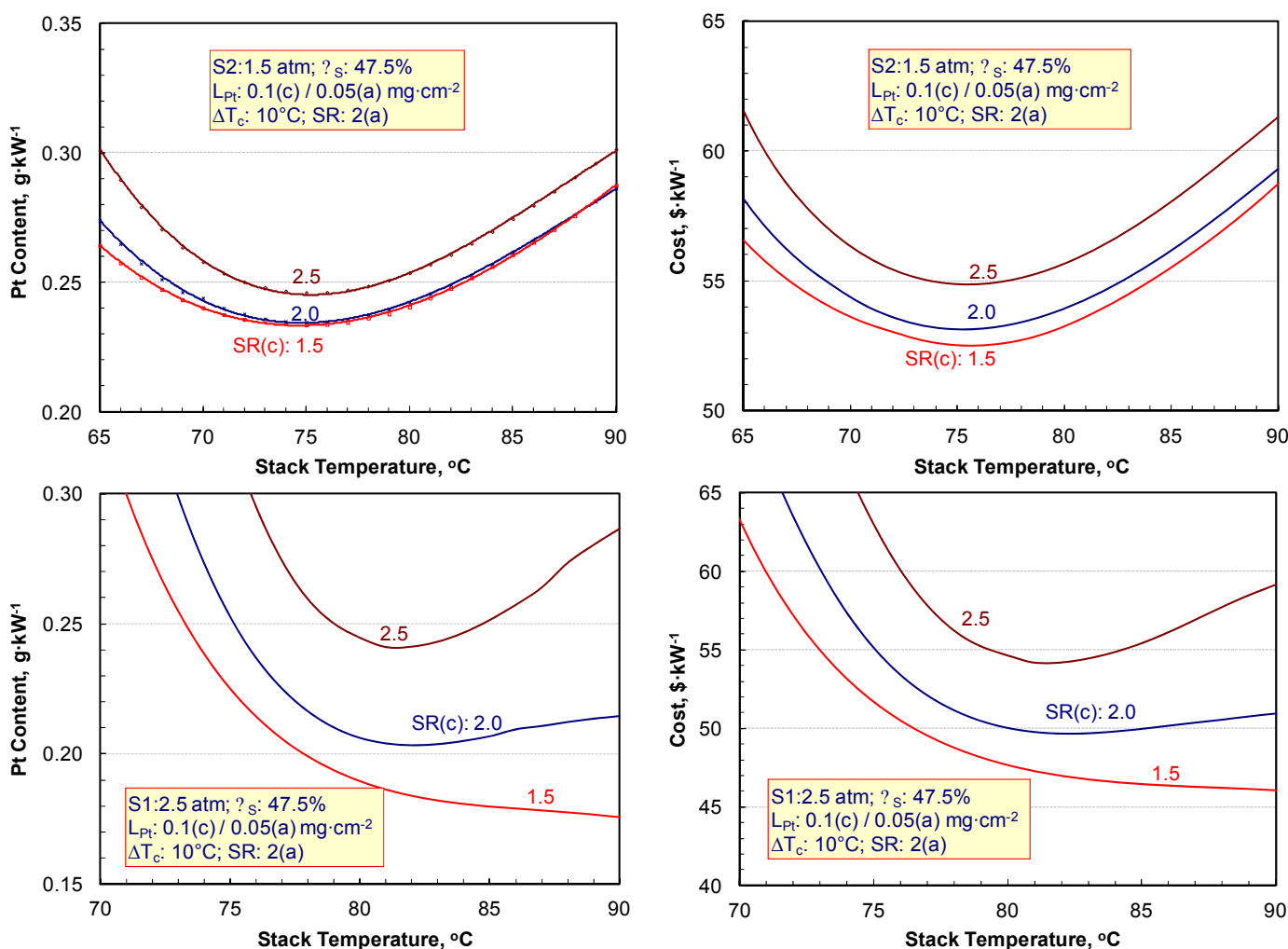
FIGURE 5. Effect of cathode stoichiometry on Pt content and system cost, 47.5% system efficiency

system efficiency (η_S) at rated power is further reduced to 40% from 45%. Also, the radiator heat load is proportional to $(1-\eta_S)/\eta_S$, so that heat rejection becomes more difficult at lower system efficiencies.

Conclusions and Future Directions

- Experimental data on 50-cm^2 single cells has been used to develop, train, and validate a multi-nodal hybrid model for fuel cells with NSTFC-based MEAs.
- Single-variable optimization studies using the hybrid model showed the dependence of the Pt content and fuel cell system cost on cell operating conditions. The optimum stack temperature was found to depend on the stack inlet pressure, increasing from 75°C at 1.5-atm stack inlet pressure to 82°C at 2.5-atm stack inlet pressure (SR$_c$ = 2). The Pt content and system cost decreased as the cathode stoichiometry was reduced from 2.5 to 1.5, with the advantage of lower parasitic

power more than compensating for the decrease in the stack power density at 2.5-atm stack inlet pressure.

- A multi-variable optimization study showed that the optimum Pt loading in the cathode catalyst decreased with decreasing stack inlet pressure or system efficiency. Over a range of 47.5–50% system efficiency, it was 0.100 mg·cm^{-2} at 1.5 atm and 0.150 mg·cm^{-2} at 2.5-atm stack inlet pressure.
- Under optimum operating conditions at 2.5-atm stack inlet pressure, the projected Pt content and system cost varied from 0.21 g·kW^{-1} and \$46.1 kW^{-1} for 47.5% system efficiency to 0.23 g.kW^{-1} and \$48 kW^{-1} for 50% system efficiency. At 1.5-atm stack inlet pressure, the projected Pt content and system increased to 0.23 g·kW^{-1} and \$52.4 kW^{-1} for 47.5% system efficiency and to 0.25 g·kW^{-1} and \$54.3 kW^{-1} for 50% system efficiency.
- In FY 2013, we will investigate the effects of alternative NSTFCs and air management system on system performance and cost.

FY 2012 Publications/Presentations

1. R.K. Ahluwalia , X. Wang, A. Lajunen, A.J. Steinbach, S.M. Hendricks, M.J. Kurkowski, and M.K. Debe, "Kinetics of Oxygen Reduction Reaction on Nanostructured Thin-Film Platinum Alloy Catalyst," J. Power Sources, 215, 77-88, 2012.

2. R.K. Ahluwalia and X. Wang, "Dynamic Performance of Automotive Fuel Cell Systems with Low Platinum Loadings," ECS Transactions, 41 (1), 293-305, 2011.

3. X. Wang, R.K. Ahluwalia, A.J. Steinbach, and M.K. Debe, "Dynamic Performance of Automotive Fuel Cell Systems with Low Platinum Loadings," 220th ECS Meeting and Electrochemical Energy Summit, Boston, MA, October 9–14, 2011.

4. Lajunen, X. Wang, and R.K. Ahluwalia, "Artificial Neural Network-Based Model for Polymer Electrolyte Fuel Cells," 5th International Conference on Polymer Batteries and Fuel Cells, Argonne, IL, August 1–5, 2011.

5. X. Wang, X. Wang, and R.K. Ahluwalia, "Effect of Air Contaminants on Performance of Polymer Electrolyte Fuel Cells," 5th International Conference on Polymer Batteries and Fuel Cells, Argonne, IL, August 1–5, 2011.

6. J. Kwon, X. Wang, R.K. Ahluwalia , and A. Rousseau, "Impact of Fuel Cell System Design used in Series Fuel Cell HEV on Net Present Value," IEEE Vehicle Power and Propulsion Conference, Chicago, IL, September 6–9, 2011.

7. R.K. Ahluwalia, X. Wang, J. Kwon, and A. Rousseau, "Drive-Cycle Performance and Life-Cycle Costs of Automotive Fuel Cell Systems," 2011 Fuel Cell Seminar & Exposition, Orlando, FL, October 31 – November 2, 2011.

References

1. M.K. Debe, "Advanced Cathode Catalysts and Supports for PEM Fuel Cells," Grant No. DE-FG36-07GO17007, FreedomCAR Technical Team Review, Detroit, MI, March 10, 2010.

2. A.J. Steinbach, C.V. Hamilton, and M.K. Debe, "Impact of Micromolar Concentrations of Externally-Provided Chloride and Sulfide Contaminants on PEMFC Reversible Stability," ECS Transactions 11(1), 889-897, 2007.

3. R.K. Ahluwalia, X. Wang, A. Lajunen, A.J. Steinbach, S.M. Hendricks, M.J. Kurkowski, and M.K. Debe, "Kinetics of Oxygen Reduction Reaction on Nanostructured Thin-Film Platinum Alloy Catalyst," J. Power Sources, 215, 77-88, 2012.

4. R.K. Ahluwalia , X. Wang, J. Kwon, and A. Rousseau, "Drive-Cycle Performance and Life-Cycle Costs of Automotive Fuel Cell Systems," 2011 Fuel Cell Seminar & Exposition, Orlando, FL, October 31 – November 2, 2011.

5. R.K. Ahluwalia, X. Wang, J. Kwon, A. Rousseau, J. Kalinoski, B. James, and J. Marcinkoski, "Performance and Cost of Automotive Fuel Cell Systems with Ultra-Low Platinum Loadings," J. Power Sources, 196, 4619, 2011.

6. M.K. Gee, "Cost and Performance Enhancement for a PEM Fuel Cell System Turbocompressor," FY 2005 Annual Progress Report, DOE Hydrogen Program, 985, 2005.

7. B.D. James, J.A. Kalinoski, and K.N. Baum, "Mass-production cost estimation for automotive fuel cell systems," DOE Hydrogen Program, Washington, DC, 2010.

8. B.D. James, J.A. Kalinoski, and K.N. Baum, "Mass Production Cost Estimation for Direct H2 PEM Fuel Cell Systems for Automotive Applications: 2009 Update," DTI Report GS-10F-0099J, January 2010.